

# Effect of Remote Phonon Scattering on Graphene-Based Devices

Z.-Y. Ong and M. V. Fischetti

Department of Materials Science and Engineering

University of Texas at Dallas, 800 W Campbell Rd., RL 10, Richardson, TX 75080

e-mail: zhunyong.ong@utdallas.edu

**Abstract**—We study the interaction between free electrons in graphene and surface optical (SO) phonon modes of the polar substrate. Electron scattering with these modes is found to be much stronger than with bulk graphene phonons. Coupled to the high sensitivity of graphene nanoribbons to line-edge roughness, we argue that graphene-based devices may exhibit a performance much lower than what may be naively expected from the high mobility observed in unsupported ideal graphene sheets.

Graphene shows much promise in nanoelectronics thanks to its excellent electrical transport properties[1]. In such applications graphene is likely to be used as armchair-edge nanoribbons (AGNRs) – in order to open a sufficiently large gap – and to be supported by an insulating substrate. The extremely strong effect of line-edge roughness on the transport properties of AGNRs has been shown before[2]. But even assuming ideally straight edges, the close proximity between the graphene and the substrate induces a significant interaction between the graphene electrons and the substrate polar phonon modes. This has been already emphasized as a strong scattering mechanism[3], [4], [5]. Here we confirm this conclusion using a more complete physical model, since dielectric screening effects on the SO modes[6] have not been investigated. Approximate models for static screening have usually been assumed [3], [4], [5], although this is inadequate when the SO frequency is higher than the plasma frequency. Another difficulty lies in the description of its transverse ( $z$ ) dielectric behavior. To circumvent these difficulties, we model graphene as an infinite thin sheet with a charge distribution that polarizes only along the longitudinal ( $x, y$ ) direction. The  $z$ -dependent effective potential  $\phi_{Q,\omega}^{scr}$  is then described by the equation:

$$\phi_{Q,\omega}^{scr}(z) = \phi_{Q,\omega}(z) + \int dz' G_Q(z, z') \rho_{Q,\omega}^{scr}(z') \quad (1)$$

where  $\phi_{Q,\omega}(z)$ ,  $G_Q(z, z')$  and  $\rho_{Q,\omega}^{scr}(z')$  are the in-plane Fourier components of the bare potential, of

the 2D Green's function, and of the dynamic polarization charge, respectively. From Eq. (1) and the continuity of the potential and the electric displacement, the equation for the dispersion relates the frequency to the wave vector and is given by:

$$\epsilon_0 + \epsilon_{ox} + [\epsilon_{ox} - \epsilon_{ox}^\infty] G_Q(0, d) \mathcal{P}_{Q,\omega} e^{-Qd} = 0$$

where  $\mathcal{P}_{Q,\omega}$  is the graphene polarization term. For a carrier density of  $n = 10^{12} \text{cm}^{-2}$ , the dispersion is shown in Fig. 1 and as expected, there are three branches resulting from the hybridization of the two SO phonon and the single plasmon branch.

We plot the scattering rates for  $n = 10^{12} \text{cm}^{-2}$  and  $n = 5 \times 10^{12} \text{cm}^{-2}$  in Figs. 2 and 3 respectively for an  $\text{SiO}_2$  substrate. We also consider the effect of a different dielectric environment of the top half by changing  $\epsilon_0 \rightarrow 4\epsilon_0$  with  $n = 10^{12} \text{cm}^{-2}$ . This simulates the immersion of the device in a high- $\kappa$  non-ionic liquid. The scattering rates are shown in Fig. 4. Compared to the case in Fig. 2, the scattering rates for the two unscreened phonon modes in the charge neutral system are reduced. However, coupled plasmon-phonon modes in the doped system induce a higher scattering rate as a result of dynamic screening of the phonon modes which is reduced in a higher-permittivity environment. A similar scattering-enhancing effect is also present in the relevant case of a high- $\kappa$  dielectric (e.g.,  $\text{HfO}_2$ ) deposited on graphene. The scattering rates for a high- $\kappa$  ( $\text{HfO}_2$ ) substrate are also plotted in Fig. 5 with  $n = 10^{12} \text{cm}^{-2}$ . They are significantly higher than those in Fig. 2. This highlights the potential drawbacks when using high- $\kappa$  dielectric material with graphene. In all cases, comparison of Figs. 2-5 with Fig. 6 – illustrating the 300 K electron-phonon scattering rates computed using the rigid-ion approximation – shows that SO-scattering is likely to vastly dominate electron transport and limit the electron mobility in supported graphene much below what may be expected for unsupported ideal graphene.

## REFERENCES

- [1] S. V. Morozov, K. S. Novoselov, M. I. Katsnelson, F. Schedin, D. C. Elias, J. A. Jaszczak, and A. K. Geim, *Giant intrinsic carrier mobility in graphene and its bilayer*, Phys. Rev. Lett. **100**, 016602 (2008).
- [2] M. V. Fischetti and S. Narayanan, *An empirical pseudopotential approach to surface and line-edge roughness scattering in nanostructures: Application to Si thin films and nanowires and to graphene nanoribbons*, J. Appl. Phys. **110**, 083713 (2011).
- [3] S. Fratini and F. Guinea, *Substrate-limited electron dynamics in graphene*, Phys. Rev. B **77**, 195415 (2008).
- [4] A. Konar, T. Fang, and D. Jena, *Effect of high- $\kappa$  gate dielectrics on charge transport in graphene-based field-effect transistors*, Phys. Rev. B **82**, 115452 (2010).
- [5] X. Li, E. A. Barry, J. M. Zavada, M. Buongiorno Nardelli, and K. W. Kim, *Surface polar phonon dominated electron transport in graphene*, Appl. Phys. Lett. **97**, 232105 (2010).
- [6] M. V. Fischetti, D. A. Neumayer, and E. A. Cartier, "Effective electron mobility in Si inversion layers in MOS systems with a high- $\kappa$  insulator: The role of remote phonon scattering" J. Appl. Phys. **90**, 4587 (2001).

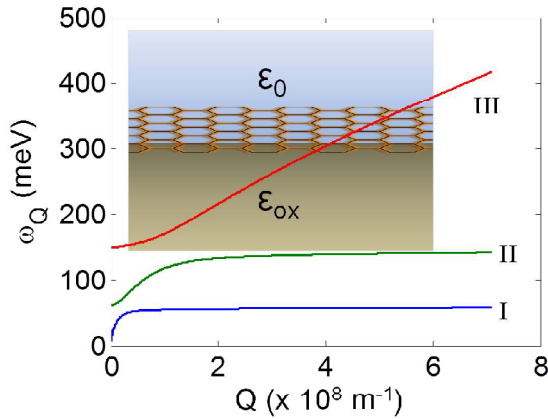


Fig. 1. Dispersion relation of the coupled plasmon-phonon modes for  $n = 10^{12} \text{cm}^{-2}$ . The blue (I) and green (II) branches are phonon-like while the red (III) one is plasmon-like. The inset illustrates the geometry considered here.

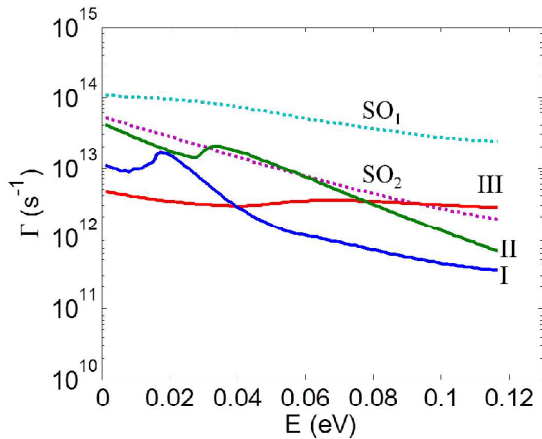


Fig. 2. Remote-phonon scattering rates for  $n = 10^{12} \text{cm}^{-2}$  for branches I to III. The scattering rates for the unscreened modes ( $\text{SO}_1$  and  $\text{SO}_2$ ) are also shown for comparison.

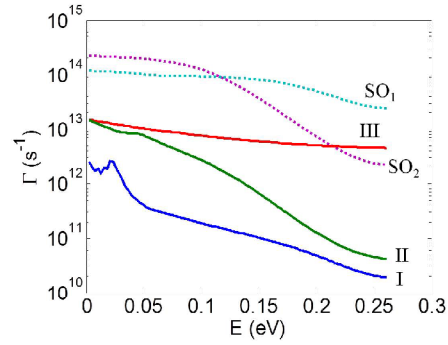


Fig. 3. Scattering rates as in the previous figure, but for  $n = 5 \times 10^{12} \text{cm}^{-2}$ .

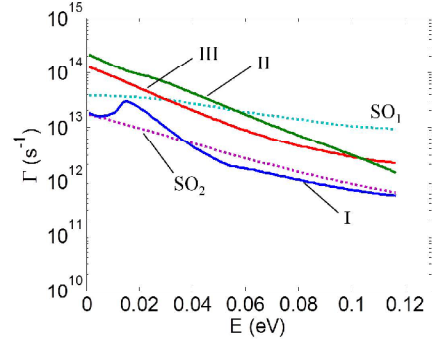


Fig. 4. Scattering rates for  $n = 10^{12} \text{cm}^{-2}$ , as in Fig. 2, but with  $\epsilon_0 \rightarrow 4\epsilon_0$ .

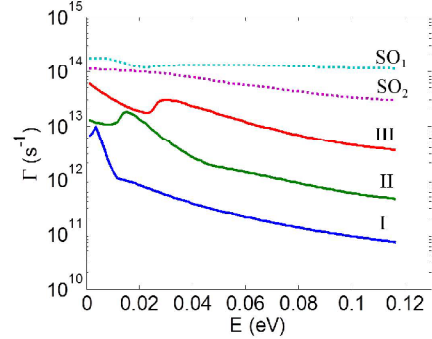


Fig. 5. Scattering rates for  $n = 10^{12} \text{cm}^{-2}$ , as in Fig. 2, but for an  $\text{HfO}_2$  substrate instead of  $\text{SiO}_2$ .

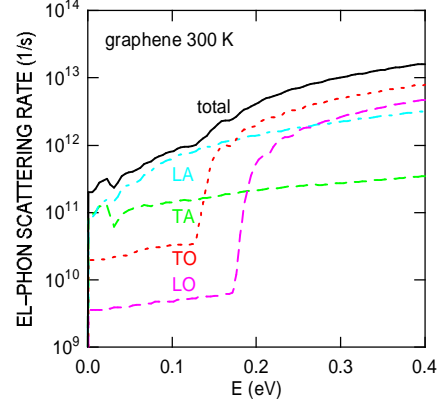


Fig. 6. Electron/graphene-bulk-phonon scattering rates at 300 K calculated using the rigid-ion approximation. Note the much smaller values than in Figs. 2-5.